AUTHOR	Schulman A, Palonen H, Lähteenlahti V, Beiranvand A, Huhtinen H, Paturi P
TITLE	Metastable ferromagnetic flux closure-type domains in strain relaxed Gd0.1Ca0.9MnO3 thin films
YEAR	2021
DOI	https://www.doi.org/10.1088/1361-648X/abbe7d
VERSION	Final Draft (AAM)

Metastable ferromagnetic flux closure-type domains in strain relaxed $Gd_{0.1}Ca_{0.9}MnO_3$ thin films

A. Schulman,[1, a)] H. Palonen,[1] V. Lähteenlahti,[1] A. Beiranvand,[1] H. Huhtinen,[1] and P. Paturi[1]

Wihuri Physical Laboratory, Department of Physics and Astronomy, University of Turku, Turku 20014, Finland

We have systematically studied the structural, electrical transport, and magnetic properties of $Gd_{0.1}Ca_{0.9}MnO_3$ (GCMO) thin films in function of thickness, which ranged from 22 nm up to 220 nm. We have found that, although no strong substrate-induced strain was detected for any thickness, a sudden change in the electric transport properties was observed when the film thickness increases above 80 nm. While thinner samples are insulating in the whole temperature range, the samples thicker than 80 nm show a clear insulator-to-metal (IMT) transition at around 100 K. The IMT coincides with the appearance of a ferromagnetic phase that is absent in the thinner samples. We associate this change in behavior with a critical film thickness that induces a sudden change in domain configuration, from in-plane domain to a closed flux-type domains with out-of-plane orientations. These out-of-plane oriented domains are meta-stable ferromagnetic in nature and result in an IMT which is accompanied by a hysteretic magnetoresistance behavior.

[a)] Electronic mail: alejandro.schulman@utu.fi

I. INTRODUCTION

Since the discovery of the colossal magnetoresistive effect (CMR) in the late 1980s, manganite-based compounds became the focus of intensive research[1,2]. In spite of intense studies in recent decades, the physical mechanism behind most magnetical and electrical properties of the manganite-based system are still poorly understood[3,4]. This is particularly true for the low bandwidth compounds where the crystal structure distortion is higher and the charge ordered phase appears at high temperatures[5]. Furthermore, there is little to no available data for the ground state of the Gd-based family due to its incompatibility with neutron diffraction techniques. Although $Gd_{1-x}Ca_xMnO_3$ was thought to be highly insulating compound with no low temperature ferromagnetic ground state in the whole phase diagram, our previous results showed that for high doping levels ($x > 0.8$) there is strong competition between metallic ferromagnetic and insulator antiferromagnetic states where an insulator to metal transition can be induced in the thin film form[6], transition that is absent from its bulk counterpart[7].

Recent *ab initio* calculations[8] show that there is a strong competition among several possible phases that have similar energies, opening the possibility to tune the films with desired properties. Generally, the physical properties of thin films are determined not only by their composition but also by their microstructure, lattice strain, and film thickness. It is well known that manganite films are intrinsically inhomogeneous[9], a feature that plays a key role in their non trivial behavior. Therefore, it is very important to understand how these factors affect the properties of the films[10].

Here, we report a systematical study of the structural, electrical transport, and magnetic properties of $Gd_{0.1}Ca_{0.9}MnO_3$ (GCMO) thin films as a function of film thickness. There are two clearly distinguished regimes in the electrical transport and magnetic properties of the films depending on their thickness. Since structural measurements show that the substrate-induced strain is negligible for all the samples, we conclude that thickness itself is the main driver behind this change of behavior. We associate a critical film thickness of ~ 80 nm with a change in domain configuration from in-plane domain to closed flux-type domains with out-of-plane orientations as explained by the domain model introduced by Kittel[11]. Through magnetotransport measurements, we were able to associate these domains with a conductive meta-stable ferromagnetic phase that can result in a insulator-to-metal transition which is

accompanied by a hysteretic magnetoresistance behavior.

II. EXPERIMENTAL DETAILS

The ceramic polycrystalline $Gd_{0.1}Ca_{0.9}MnO_3$ (GCMO) target for pulsed laser deposition (PLD) was prepared by a solid state reaction method[12]. Initially, Gd_2O_3 oxide was calcined at 1300 °C for 12 h in air and, on the other hand, $CaCO_3$ and MnO_2 were dried at 200 °C in air. The stoichiometric amounts were thoroughly ground, pressed to a pellet and calcined at 750 °C for 60 h in air. To finalize the target, the further grinding–sintering process at 1300 °C for 24 h in air was repeated twice.

A series of epitaxial GCMO thin films with different thicknesses were deposited by PLD on single crystal $SrTiO_3$ (100) substrates using a XeCl excimer laser ($\lambda = 308$ nm) with an energy density of 2.0 J/cm^2 and a frequency of 5 Hz[13,14]. The different number of laser pulses was utilized to vary the film thickness. The target-to-substrate distance was 32 mm and the substrate was attached to an Inconel plate with silver paste and then heated with a PVD Product's IR diode laser. The deposition temperature was 700 °C and the deposition was done in flowing O_2 at 23 Pa. After the deposition, an oxygenation step of 10 min at 700 °C in 1 atm of pure O_2 was made for all the films before cooling them down to room temperature. Final film thicknesses, which ranged from 22 nm up to 220 nm, were determined from the positions of the interference minima[15] of x-ray reflectivity measurements (XRR) (Fig. 1(a)) for the thinner films ($<$ 100 nm). In contrast, scanning electron microscopy (SEM) was utilized to measure the thickness of the thicker ones, since XRR measurements do not show any fringes for high thicknesses.

The phase purity and the film crystallinity were studied by x-ray diffraction (XRD) using a Panalytical Empyrean diffractometer equipped with a PixCel 3D detector. Electrical transport properties were measured in a 9 T Quantum Design physical properties measurement system (PPMS) utilizing four Au probe electrodes deposited by DC-magnetron sputtering on top of the films with a distance between the electrodes of 250 μm. Gold was chosen as an electrode material because it forms an ohmic junction with the GCMO samples, if low enough bias is applied[12]. Magnetization of the samples was measured by a Quantum Design MPMS SQUID magnetometer. In addition to the zero field cooled (FC) and field cooled (ZFC) temperature scans in 50 mT, hysteresis loops between -5 T and 5 T were measured

at 10 K.

III. RESULTS AND DISCUSSION

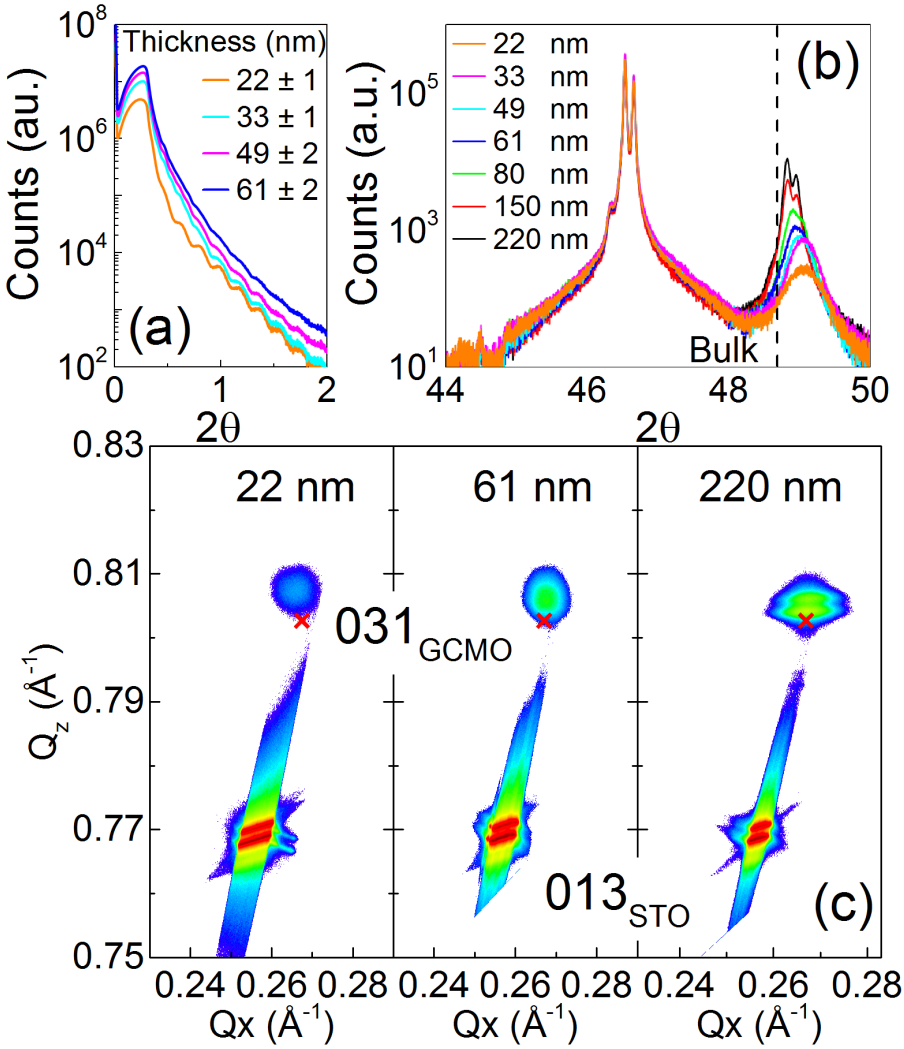

FIG. 1. (a) XRR data of the thinner films with their respective calculated thicknesses. The curves are shifted for clarity. (b) θ - 2θ scans of all GCMO thin films around the (020) Bragg reflection. (c) Reciprocal space map around their (031) Bragg reflection for films with thickness (from left to right): 22 nm , 61 nm, 220 nm. The red cross marks indicate the measured bulk value.

The good structural qualities of the thin films were confirmed by XRD measurements. A broad XRD 2θ scan indicates that all films are single phase and fully textured with $(0k0)$ as the out-of-plane direction with no detectable mixed phases present. The epitaxy of the films

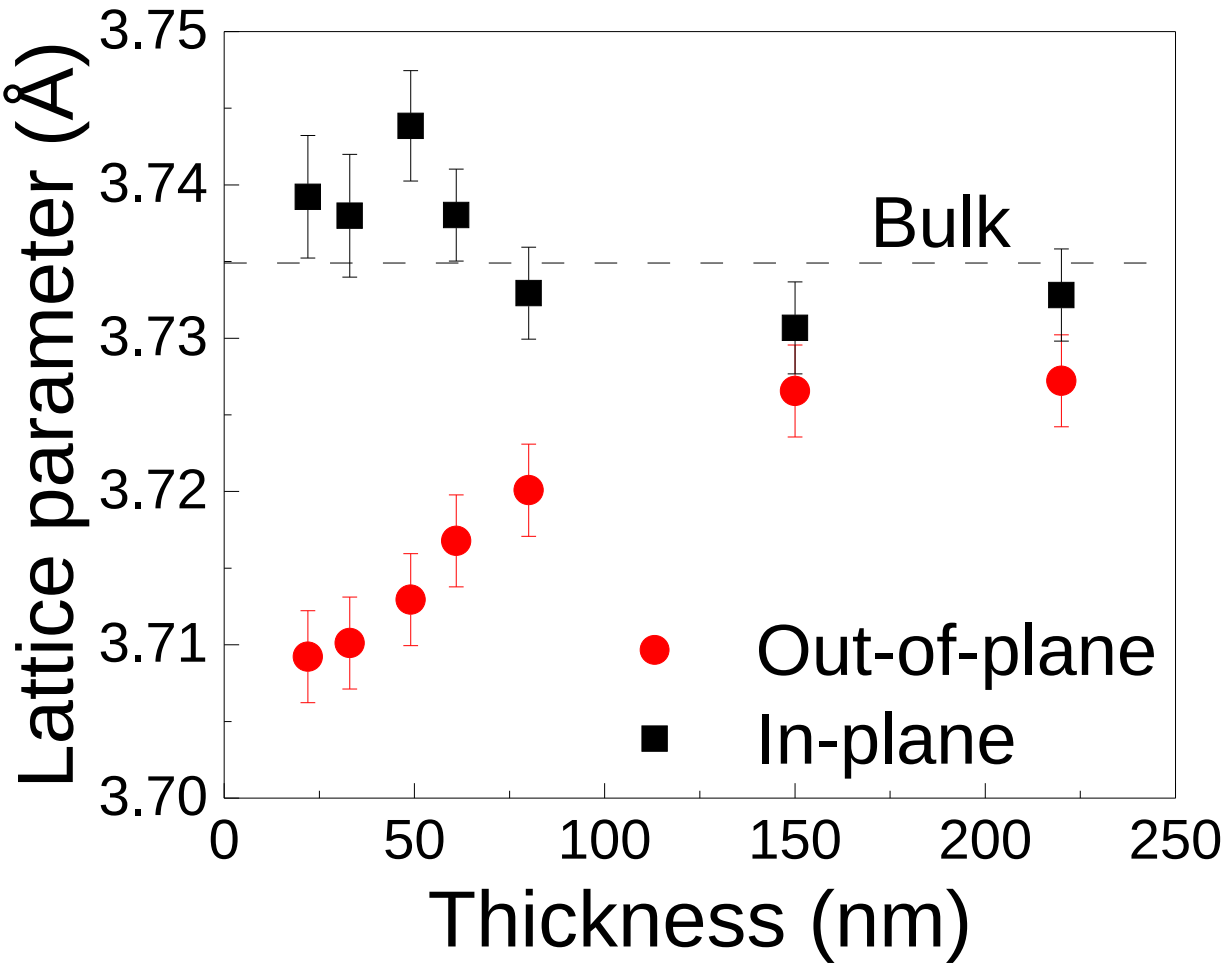

FIG. 2. (a) Evolution of both the in-plane and out-of-plane lattice parameters of the GCMO films in function of thickness. The dashed line represents the value of the pseudocubic lattice parameter of the bulk target calculated from measurements reported in Ref. [7]

was further corroborated by ϕ-scans that show four peaks with an equal separation of 90° as expected (not shown). θ - 2θ scans around the (020) Bragg reflection in the pseudocubic lattice are presented in Fig. 1(b), where an enhancement in the relative intensity of the film peaks with increasing film thickness is seen. The increase in the peak intensity is expected since we increased the quantity of the diffracting material by increasing the film thickness. Additionally, when the thickness of the film is increased from 22 to 220 nm, a narrowing of the peak can be clearly observed to the point were one can distinguish Kα_1 and Kα_2 peaks on the thicker films. These effects were previously reported for epitaxial films in other manganite-based compounds and have been attributed to finite-size effects[16]. A smooth evolution of the out-of-plane lattice parameter towards the bulk value can also be discerned.

This out-of-plane evolution of the lattice parameter is usually taken as an indicator of a change in the strain, that is induced by the mismatch between the substrate and film lattice parameters, which relaxes with the increase in film thickness[17]. To further assess the strain state of the samples, we performed reciprocal space mappings (RSM) around the GCMO (031) reflection. In Fig. 1(c), we present the results for three samples: the thinnest, a middle range, and the thickest one, but all the samples display similar results. The first thing we can observe is that none of the samples are fully aligned with the substrate along the Q_x direction, indicating that none of the samples are fully strained. In contrast, all the samples align well with the bulk value, marked with a red cross. The evolution of the lattice parameters in both the in-plane and out-of-plane directions are presented in Fig. 2, and it shows more clearly the evolution of the out-of-plane lattice parameter observed in Fig. 1(b). The other direction also shows a small shift of the lattice parameters, not towards the bulk values but towards a more tetragonal structure, which keeps the unit cell volume of all thicknesses approximately equal at (207.6 ± 0.5) Å^3. These results indicate that although there is a small relaxation of the in-plane strain with increasing thickness, none of the samples are clamped to the substrate. Furthermore, by utilizing the well-known M–B theory[18] of strain relaxation, we can approximate the critical thickness (h_c) for the onset of strain relaxation by misfit dislocations as

$$h_c = \frac{b}{8\pi f}\frac{(1-\nu cos^2\theta)}{(1+\nu)cos\lambda}\ln\left(\frac{\beta h_c}{b}\right), \tag{1}$$

where b is the magnitude of the Burgers vector for dislocations, ν is the average Poisson ratio (≈ 0.3)[17], f is the misfit strain between the film and substrate, θ is the angle between the Burgers vector and dislocation lines, λ is the angle between the Burgers vector and line that lies within the interface and in a plane normal to the dislocation line, and β the cutoff radius of the dislocations, which we estimated to be close to 4 based on reports in similar systems[19,20]. If we assume a burgers vector of the type $\langle 1\ 1\ 0\rangle$, as it is the most common in these kinds of systems[21–23], we obtained a critical thickness of around 12 nm, which roughly corresponds to 15 unit cells. This is not an usual result since many studies have shown that in manganite-based thin films, a thickness between 10 nm and 20 nm[16,17,24] is the upper threshold to observe strong strain effects and our thinnest film is 22 nm.

In spite of the lack of observed strong substrate-induced strain, the effect of the thickness in the physical properties of the films is evident when observing their electrical transport

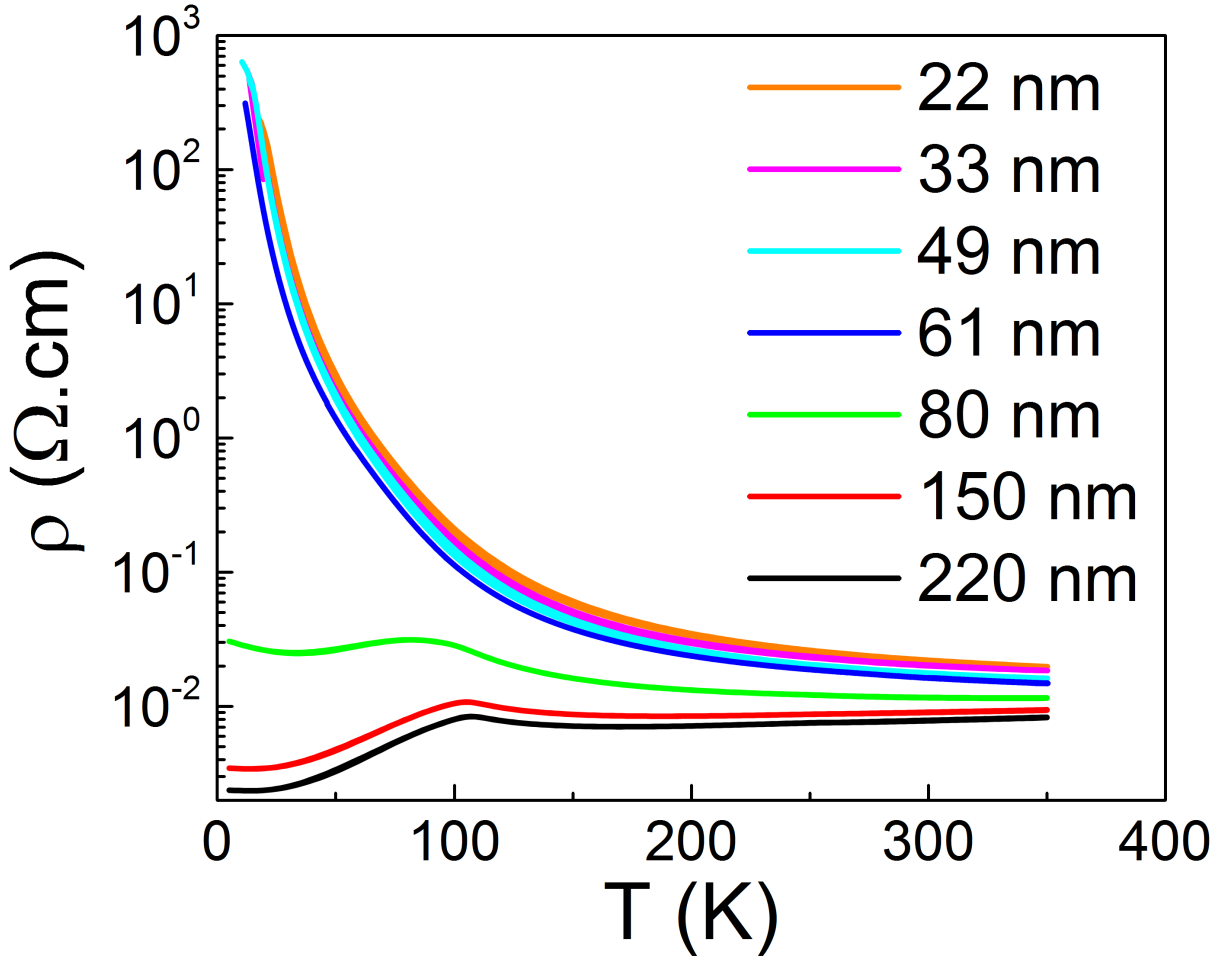

FIG. 3. Temperature dependence of the four wire resistivity for the GCMO films of different thicknesses.

characteristics. Fig. 3 shows the evolution with film thickness of the resistivity versus temperature curves. The resistivity increases continuously as the film thickness is reduced and two different regimes can be distinguished. At low thicknesses, the GCMO films have relatively large resistivity and an insulating behavior in the whole temperature range. When the thickness increases above 80 nm, an insulator-to-metal transition (IMT) appears at low temperatures. The emergence of the IMT coincides with a transition to a ferromagnetic phase (see Fig. 5). For the manganese oxide-based films, is it well known that the transition temperature of the IMT is related to the Mn–O–Mn angle through the double exchange mechanism, which is heavily influenced by a combination of substrate-induced strain, defects, and film thickness[17,25]. The transition temperature (T_c) shows a small evolution with the thickness of the films, shifting from (101 ± 1) K for the 80 nm film to (108 ± 1) K for the

220 nm film, similar to systems over the upper threshold for observing strain effects[26]. It is also worth noting that the appearance of the IMT is quite abrupt and the observed evolution of the lattice parameter is smooth. This, coupled with the fact that we observed negligible strain by XRD, strongly indicates that the transition is purely triggered by thickness as opposed to substrate-induced strain.

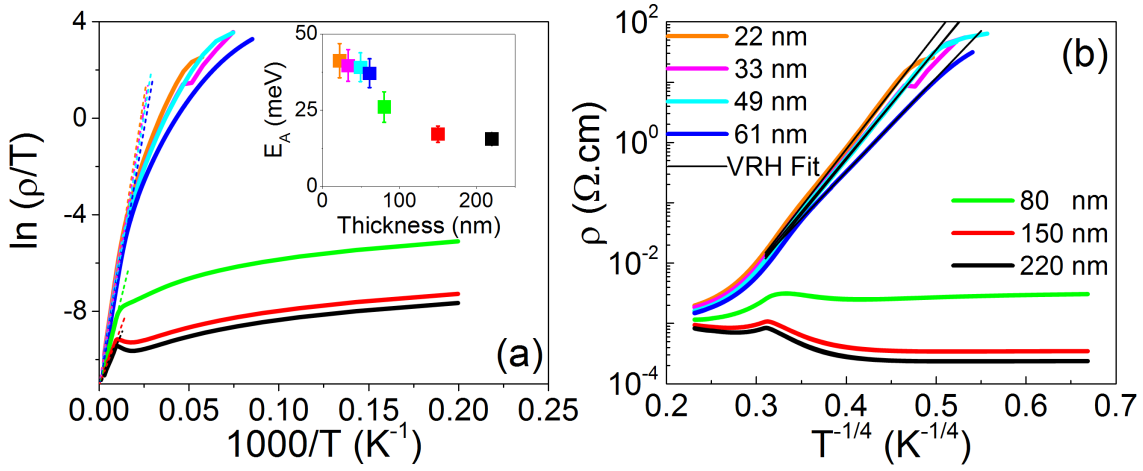

FIG. 4. (a) Arrhenius-type plot ($\ln(\rho/T)$ vs. $1/T$) for all the samples. Dashed lines are fittings to the experimental data with the small polaron hopping model. Inset: Hopping energies obtained from the fitting. (b) Semilog plot of the resistivity vs. $T^{-1/4}$, indicating that Mott VRH is the dominant conduction mechanism in the thinner films at lower temperatures. The legend in (b) applies to both graphs.

To further explore the effect of thickness, we studied the electrical conduction mechanism in more depth. We found that for all the samples in their high temperature insulating state, the conduction mechanism is dominated by the adiabatic Emin-Holstein model[27], better known as the adiabatic small polaron hopping model. This model gives a resistivity of the form $\rho(T) = \rho_0' T \exp(E_A/k_B T)$, where ρ_0' is a temperature independent pre-factor, k_B the Boltzmann constant and E_A the hopping energy. It is a very common thermally activated model, often observed on manganites in their high temperature paramagnetic phase. It is related to the coupling of the electrons with the elastic lattice polarons, which are originated from the strong Jahn-Teller effect of Mn^{3+} ions[28]. We calculated the polaron hopping energies by replotting the resistivity curves as $\ln(\rho/T)$ vs. $1/T$ (Fig. 4(a)), which yields a straight line where E_A can be directly obtained from the slope. We observe a subtle

decrease in the hopping energies with increasing thickness (see inset of Fig. 4(a)), which is compatible with the decrease in the resistivity values observed. This reduction in E_A can have many origins and is usually explained in terms of magnetic disorder caused by interfacial phase separation, localized chemical non-stoichiometry, and oxygen vacancies[29].

Interestingly, the thinner films that do not have an IMT show a change in the conduction mechanism at similar temperatures than their thicker counterparts. For these samples, the conduction mechanism at low temperatures is dominated by a Mott-type variable range hopping (VRH) conduction mechanism. As a result, the resistivity below the transition shows an inverse relationship with the temperature expressed as $\rho = \rho_0 \exp\left(\frac{T_0}{T}\right)^{0.25}$, where ρ_0 is a prefactor, T_0 is the characteristic VRH temperature, which is inversely proportional to the density of states near the Fermi level. The good fit with the model can be observed in Fig. 4(b). This conduction mechanism is typical of disordered systems and is an indicator of a change in the magnetization order at the crossover temperature.

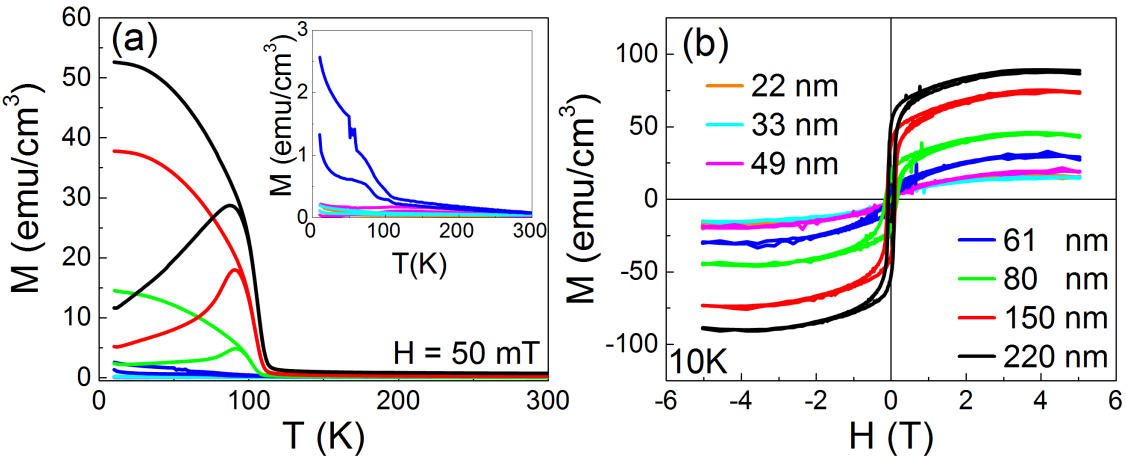

FIG. 5. (a) The ZFC-FC curves of the GCMO films fabricated with different thicknesses. The inset is a zoom around $M = 0$ to show the thinner films in greater detail. (b) The M - H curves of the films measured at 10 K. The legend in (b) applies to both graphs.

The magnetic properties of the GCMO films are shown in Fig. 5, where the two regimes observed in the transport properties can also be discerned. ZFC-FC curves are shown in Fig. 5(a). Thinner films exhibit a small increase in M at around 100 K, which is the temperature where the crossover of conduction mechanisms appears in transport measurements. This suggests that the small increase in M arises from a phase transition from an insulating

paramagnetic phase to an antiferromagnetic insulator. Meanwhile, thicker films exhibit a sharp transition with a ferromagnetic-like behavior at low temperatures. The transition temperature follows a similar behavior of the one observed for the IMT. Though samples present signs of ferromagnetic interactions, the exact nature of the magnetic ordering is certainly more complicated. Indeed, the magnetization curves show the typical λ shape characteristic of glassy systems, resulting from competing magnetic interactions that coexist on both sides of the magnetic transition[30]. Furthermore, recent *ab-initio* calculations[8] for this particular system predict very similar energies for different competing magnetic orders such as FM and A-AFM, or even ferrimagnetism, making the phase coexistence scenario

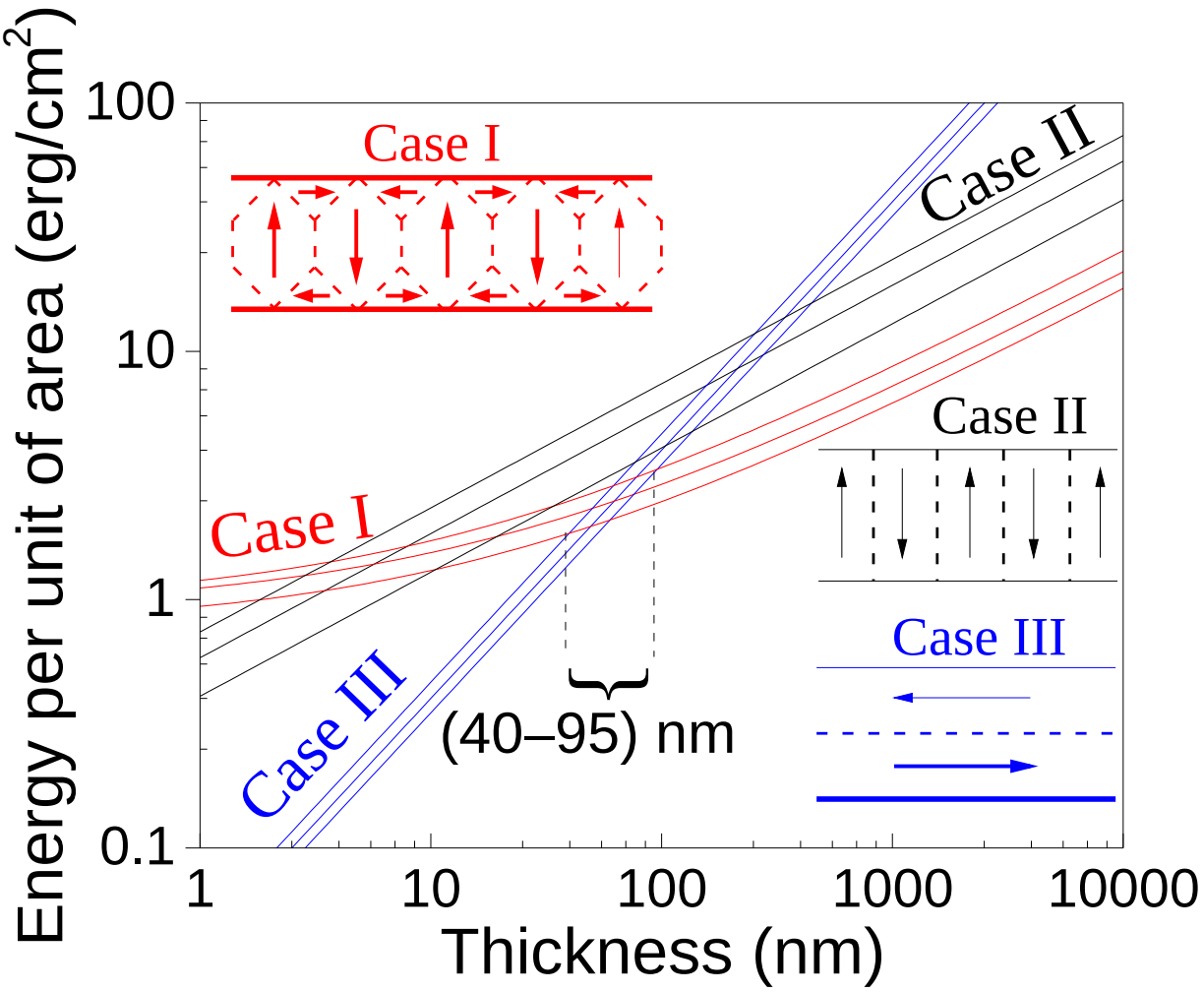

FIG. 6. Thickness dependence of the free energy for the schematized domain configurations. The energy is presented along with the confidence bands (in thinner lines) to obtain a more reliable result since some parameters are very sensitive to the fabrication processes.

the more plausible one. The hysteresis loops (M - H curves) reveal a similar picture (Fig. 5(b)). As thickness decreases, the saturation magnetization of the sample also decreases. In contrast, enhanced coercivity was observed from 80 to 1600 Oe with thickness changing from 220 nm to 80 nm. Unlike the thicker films, thinner films show no hysteresis, reinforcing the theory that there is no ferromagnetic minority phase present for these thicknesses.

The sharp change in behavior with thickness can be explained by a change in the magnetic domain orientation as explained by the classical Kittel's model[11]. In this model, the free energy F in thin magnetic samples is written as

$$F = F_a + F_W + F_m = \rho_a V_a + \sigma_W S - \frac{1}{2} \int (M \cdot H) dV, \tag{2}$$

where F_a, F_W, and F_m are the anisotropy energy, domain wall energy and the magnetic field energy, respectively. F_a is related to the anisotropy energy density (ρ_a) and the volume of the domains (V_a), while F_W is linked to the surface energy per unit area (σ_W) and the total area of the domain boundary (S). Meanwhile, F_m is dictated by the magnetic field and the magnetization. In the manganite films, F_a is mainly due to the perpendicular magnetic anisotropy. Kittel calculated the total free energy F for three types of domain configurations in thin films: (I) flux closure-type domains, (II) out-of-plane oriented domains, and (III) in-plane oriented domains. The configuration of the domains is schematized in Fig. 6 along with their calculated free energy in function of film thickness. For the case (I), $F_m = 0$ and the minimum of the total free energy can be approximately expressed as

$$F_{min} \approx F_a + F_W \approx \sigma_W (2\sqrt{2} - 1) + \sqrt{\sigma_W T \rho_a}, \tag{3}$$

where T is the thickness of the film. In case (II) where all the domains are oriented in the out-of-plane direction, the anisotropy energy F_a is zero and

$$F_{min} \approx F_W + F_m \approx 2M_s \sqrt{1.7 \sigma_W T}, \tag{4}$$

with M_s the saturation magnetization. In case (III), the film is mangetized in-plane, hence the principal contribution to the energy comes from the anisotropy and

$$F_{min} \approx F_a \approx \rho_a T. \tag{5}$$

We applied this model to our samples by utilizing values reported for other similar manganite-based films[31–39]. We estimated the domain wall energy to be in a range between 0.35 and 0.45 erg/cm^2, $\rho_a = (3.5 \times 10^5 \pm 1 \times 10^5)$ erg/cm^3 and the saturation

magnetization between 50 and 250 emu/cm^3. Our results are displayed in Fig. 6 and show that in-plane magnetic domains are dominant at low thicknesses and they are replaced by flux closure domains with out-of-plane oriented domains at higher thicknesses. The critical thickness was calculated to be in the range of 40 to 95 nm, which is in agreement with the change of behavior observed in our samples and with the results reported by Dho and Hur for LSMO samples[32]. The critical thickness range depends mostly on the utilized value of the anisotropy energy density, which itself depends greatly on the substrate-induced strain. Given that our samples are not strained, the transition value can be effectively tuned utilizing strain engineering if there is a requirement to do so.

In fact, magnetic textures such as magnetic bubbles and magnetic stripe domains are known to form in similar compounds[35,37,38]. In this context, a bubble is often described as a rod-like domain with out-of-plane magnetization, which is embedded in an antiparallel magnetization background and separated with a cylindrical Bloch wall. This is very similar to the flux closure-type domains described by Kittel. Furthermore, these magnetic domains can also show interesting topological spin textures and are usually referred as skyrmionic bubbles[40]. Indeed, skyrmion systems are being intensively studied with the goal to create high-performance spin devices. In this context, it is important to fully understand which factors affect their formation and any thickness effect will need to be taken into account, if viable devices are to be obtained. It is worth noting that we cannot claim at this moment that our particular system presents this kind of magnetic topology, just that the change in the magnetic domain orientations with thickness is compatible with the appearance of magnetic bubbles. More studies are being carried out to determine the details of the magnetic domain topology in this system.

The coexistence between conductive and insulating phase for thicker samples becomes more evident when studying the magnetoresistance (MR) response as function of thickness and temperature; results that are summarized in Fig. 7. Here, the MR ratio is defined as $\mathrm{MR} = [R(9T) - R(0)]/R(0) \times 100\%$. Above T_c (Fig. 7(a)), all samples show a small negative MR effect, between 2% and 3%, typical of manganite systems where MR scales with the square of the magnetization[41]. Below T_c (Fig. 7(b)), a completely different behavior was observed depending on the thickness of the samples. Thinner samples still show a quadratic response although with a much higher MR value and no signs of hysteresis, while thicker samples display a completely different behavior where the MR is hysteretic and exhibits

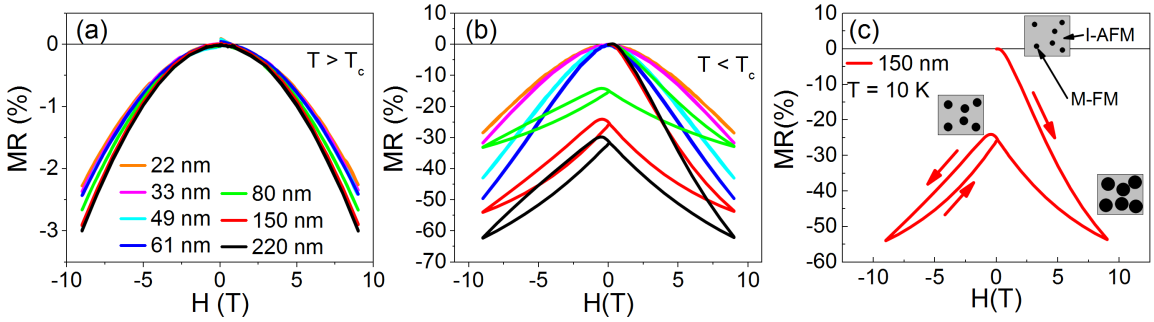

FIG. 7. (a) Magnetic field dependence of the magnetoresistance for temperatures above (a) and below (b) T_c. (c) Detail of the magnetoresistance for the 150 nm thick sample along with the schematics of how the magnetic field affects the nucleation of the metallic ferromagnetic phase (M-FM) in an insulating antiferromagnetic matrix (I-AFM). The legend in (a) applies to (a) and (b).

distinct differences between the virgin curve and subsequent field cycles (an example curve is shown in Fig.7(c)). This effect is often observed when a metastable conductive phase is induced by the external magnetic field while the rest of the material remains in the stable insulating phase[42]. For our samples, this conductive phase was found to be ferromagnetic in nature. This metallic phase is arrested, meaning that it possesses a glass-like behavior and is typically called magnetorelaxor, which has been widely reported in other manganite-based systems[43,44], albeit usually at half doping. As mentioned, our GCMO samples are in the vicinity of the phase boundary between several competing phases at low temperatures. This means that when we reach T_c, the MR starts to increase, indicating the beginning of cluster nucleation as schematized in Fig.7(c). The external magnetic field both increases the volume and aligns the spins in the metallic-FM clusters. When the distance between the domains is small enough, the insulating antiferromagnetic phase acts as the barrier in the spin polarized tunneling FM-insulating-FM structures resulting in the observed MR effect, similar to the effect of grain boundaries in polycrystalline LSMO[45] and CCMO[44] films. Reversing the magnetic field only partially restores the sample to the original AFM phase, thus the MR exhibit the observed non-volatile behavior. This non-volatile behavior could be of interest for memory applications, especially if it can be coupled with the control mechanism for the creation/movement of magnetic bubbles. Further studies are necessary to shed light on the origin of the magnetorelaxor-like behavior and how to control it.

IV. CONCLUSION

In summary, we have shown that the magnetical and electrical transport properties of $Gd_{0.1}Ca_{0.9}MnO_3$ thin films are thickness dependent, even in the absence of significant substrate-induced strain. The thinner films below 80 nm show an insulator behavior with no signs of ferromagnetism, while the thicker samples exhibit an insulator-to-metal transition at around 100 K, which is accompanied with a magnetorelaxor-like behavior. The critical thickness for the appearance of the ferromagnetic phase can be successfully explained by Kittel's model indicating a shift from in-plane domains to bubble type domains with out-of-plane magnetization. These magnetic bubbles may possess interesting topological properties that are worth exploring in more detail.

ACKNOWLEDGMENTS

The authors wish to thank the Jenny and Antti Wihuri Foundation and the Academy of Finland grant no. 308285. A.B. also acknowledges the Väisälä foundation and V.L. the University of Turku Graduate School for general resources and finance.

REFERENCES

[1]Y. Tokura, *Colossal Magnetoresistive Oxides*, (New York: Gordon and Breach Science) (2004).

[2]M. B. Salamon and M. Jaime, *Rev. Mod. Phys.* **73**, 583 (2001).

[3]Y. Tokura, *Rep. Prog. Phys.* **69**, 797 (2006).

[4]K. Dörr, *J. Phys. D: Appl. Phys.* **39**, 125 (2006).

[5]Y. Tomioka and Y. Tokura, *Phys. Rev.* B **70**, 014432 (2004).

[6]A. Schulman, A. Beiranvand, V. Lähteenlahti , H. Huhtinen, and P. Paturi, *J. Magn. Magn. Mater.* **498**, 166149 (2020).

[7]A. Beiranvand, J. Tikkanen, H. Huhtinen, and P. Paturi, *J. Alloys Comp.* **720**, 126 (2017).

[8]H. Ben Hamed, M. Hoffman, W. A. Adeagbo, A. Ernst, W. Hegert, T. Hynninen, K. Kokko, and P. Paturi, *Phys. Rev.* B **99**, 14428 (2019).

[9]T. Becker, C. Streng, Y. Luo, V. Moshnyaga, B. Damaschke, N. Shannon, and K. Samwer, *Phys. Rev. Lett.* **23** 237203 (2002).

[10]E. Dagotto, T. Hotta, and A. Moreo, *Phys. Rep.* **344** 1 (2001).

[11]C. Kittel, *Phys. Rev.* **70** 965 (1946).

[12]P. Paturi, J. Tikkanen, and H. Huhtinen, *J. Magn. Magn. Mater.* **432**, 164 (2017).

[13]A. Beiranvand, J. Tikkanen, H. Huhtinen, and P. Paturi, *J. Magn. Magn. Mater.* **469**, 253 (2019).

[14]H. Palonen, H. Huhtinen, M. A. Shakhov, and P. Paturi, *Supercond. Sci. Technol.* **26**, 045003 (2013).

[15]T. C. Huang, R. Gilles, and G. Will, *Thin Solid Films* **230**, 99 (1993).

[16]A. de Andres, J. Rubio, G. Castro, S. Taboada, J. L. Martinez, and J. M. Colino, *Appl. Phys. Lett.* **83**, 713 (2003).

[17]F. Sandiumenge, J. Santiso, L. Balcells, Z. Konstantinovic, J. Roqueta, A. Pomar, J. P. Espinós, and B. Martínez, *Phys. Rev. Lett.* **110**, 107206 (2013).

[18]J. W. Matthews and A. E. Blakeslee, *J. Cryst. Growth* **27**, 118 (1974).

[19]L. Qiao, T. C. Droubay, T. Varga, M. E. Bowden, V. Shutthanandan, Z. Zhu, T. C. Kaspar, and S. A. Chambers, *Phys. Rev.* B **83**, 085408 (2011).

[20]W. S. Choi, J.-H. Kwon, H. Jeen, J. E. Hamann-Borrero, A. Radi, S. Macke, R. Sutarto, F. He, G. A. Sawatzky, V. Hinkov, M. Kim, and H. N. Lee, *Nano Lett.* **12**, 4966 (2012).

[21]S. C. Jain , A. H. Harker, and R. A. Cowley, *Phil. Mag.* A **75**, 1461 (1997).

[22]C. L. Canedy, H. Li, S. P. Alpay, L. Salamanca-Riba, A. L. Roytburd, and R. Ramesh, *Appl. Phys. Lett.* **77**, 1695 (2000).

[23]S. Venkatesan, A. Vlooswijk, B. J. Kooi, A. Morelli, G. Palasantzas, J. T. M. De Hosson, and B. Noheda, *Phys. Rev.* B **78**, 104112 (2008).

[24]M. Huijben, L. W. Martin, Y.-H. Chu, M. B. Holcomb, P. Yu, G. Rijnders, D. H. A. Blank, and R. Ramesh, *Phys. Rev.* B **78**, 094413 (2008).

[25]D. Gutiérrez, G. Radaelli, F. Sánchez, R. Bertacco, and J. Fontcuberta, *Phys. Rev.* B **89**, 075107 (2014).

[26]D. Fuchs, T. Schwarz, O. Morán, P. Schweiss, and R. Schneider, *Phys. Rev.* B **71**, 092406 (2005).

[27]D. Emin and T. Holstein, *Ann. Phys.* **53**, 439 (1969).

[28]A.-M. Haghiri-Gosnet and J.-P. Renard, *J. Phys. D: Appl. Phys.* **36**, 127 (2003).

[29]R. Prasad, H. K. Singh, M. P. Singh, W. Prellier, P. K. Siwach, and A. Kaur,*J. Appl. Phys.* **103**, 08396 (2008).

[30]M. Itoh, I. Natori, S. Kubota, and K. Motoya, *J. Phys. Soc. Jpn.* **63**, 1486 (1994)

[31]K. Steenbeck, T. Habisreuther, C. Dubourdieu, and J. P. Sénateur, *Appl. Phys. Lett.* **80**, 3361 (2002).

[32]J. Dho and N. H. Hur, *J. Magn. Magn. Mater.* **318**, 23 (2007).

[33]J. M. D. Coey, *Magnetism and magnetic materials*, (Cambridge University Press) (2010).

[34]A. Kotani, H. Nakajima, K. Harada, Y. Ishii, and S. Mori, *Phys. Rev.* B **95**, 144403 (2017).

[35]T. Asaka, S. Mori, Y. Horibe, K. Takenaka, X. Z. Yu, T. Nagai, K. Kimoto, T. Hirayama, and Y. Matsui, *Phys. Rev.* B **83**, 174401 (2011).

[36]M. Nakamura, D. Morikawa, X. Yu, F. Kagawa, T. Arima, Y. Tokura, and M. Kawasaki, *J. Phys. Soc. Jpn.* **87**, 074704 (2018).

[37]L. Vistoli, W. Wang, A. Sander, Q. Zhu, B. Casals, R. Cichelero, A. Barthélémy, S. Fusil, G. Herranz, S. Valencia, R. Abrudan, E. Weschke, K. Nakazawa, H. Kohno, J. Santamaria, W. Wu, V. Garcia, and M. Bibes, *Nat. Phys.* **15**, 67 (2019).

[38]T. Nagai, M. Nagao, K. Kurashima, T. Asaka, W. Zhang, and K. Kimoto, *Appl. Phys. Lett.* **101**, 162401 (2012).

[39]T. Koyama, Y. Togawa, K. Takenaka, and S. Mori, *J. Appl. Phys.* **111**, 07B104 (2012).

[40]X. Yu, Y. Tokunaga, Y. Taguchi, and Y. Tokura, *J. Appl. Phys.* **111**, 07B104 (2012).

[41]J. Fontcuberta, B. Martínez, A. Seffar, S. PiÃśol, J. L. García-MuÃśoz, and X. Obradors, *Phys. Rev. Lett.* **76** 1122 (1996).

[42]S. K. giri and t. K. Nath, *J. Appl. Phys.* **115**, 053902 (2014).

[43]Y. Ogimoto, M. Izumi, T. Manako, T. Kimura, Y. Tomioka, M. Kawasaki, and Y. Tokura, *Appl. Phys. Lett.* **78**, 3505 (2001).

[44]P. -H. Xiang, H. Yamada, A. Sawa, and H. Akoh, *Appl. Phys. Lett.* **94**, 062109 (2009).

[45]X. Wang, C. Jin , P. Wang, X. Pang, W. Zheng, D. Zheng, Z. Li , R. Zheng , and H. Bai, *Appl. Phys. Lett.* **115**, 182405 (2019).